RELIABLE SEALS FOR TURBOMACHINES: NUMERICAL ANALYSIS OF THE EFFECTS OF COMPRESSIBLE FLUID FLOW THROUGH POROUS MATERIALS AND NARROW GAPS

S. Schoar, H. J. Dohmen, F.-K. Benra

University of Duisburg-Essen, Chair of Turbomachinery, Duisburg, Germany
Schaham.Schoar@uni-due.de

ABSTRACT

Leakage between rotating and stationary parts in turbomachines has a strong impact on performance and reliability. So, the demand for robust and reliable sealing solutions is high. Under challenging operating conditions, dry gas seals and aerostatic gas seals are used to avoid high leakage rates and high friction losses.

Generally, an aerostatic seal is pressurized by several holes distributed over the sealing. As a result, a gap of a few micrometers between the slip ring and rotating ring arises. This operation is very similar to that of an air bearing. However, it has been shown in the past that the use of porous materials makes the flow film more stable regarding any force effects. The major difference between an aerostatic seal and an air bearing is that the porous layer of an air bearing is mounted in the housing in a fixed manner, while it is freely movable in a gas seal and thus adjusts autonomously with respect to its force equilibrium. These characteristic properties impact the entire operational behavior of a seal.

In this paper a numerical investigation is undertaken to check the feasibility of an aerostatic gas seal with a porous ring. By using MATLAB, a design tool is developed to quickly calculate the pressure profile in the gap and the operational behavior of the seal. Special focus is put on the control of the permeability (pore distribution) and the geometric size of the porous material and its impact on the gap flow. The model is based on the assumption of Darcy's law in the porous part and a laminar viscous flow field with isothermal conditions in the gap. Using a test bench, the numerical analysis is validated. In addition, the pressure distribution in the gap is shown when lifting the porous ring for different permeability distributions.

KEYWORDS

MICRO GAP, PERMEABILITY, PERMEABILITY DISTRIBUTION EFFECT

NOMENCLATURE

A	area	[m^2]	r	radial direction	[mm]
F	force	[N]	r_a	outer radius	[mm]
$F_{o,sp}$	force relationship	[N]	r_i	inner radius	[mm]
F_s	spring force	[N]	t	time	[s]
K	permeability	[m^2]	v, w	component of velocity in r, z direction	[-]
M	matrix	[-]	r, z	cartesian coordinates	[-]
R	specific gas constant	$\left[\frac{J}{kg\,K}\right]$	ε	convergence accuracy	[-]
T	temperature	[K]	η	dynamic viscosity of fluid	[Pa s]

h	gap height	[µm]	ρ	density of fluid	$\left[\frac{kg}{m^3}\right]$
n	iteration step	[-]	φ	circumferential direction	[-]
p	pressure	[bar]			

INTRODUCTION

In order to keep the efficiency of compressors at a high level, the shaft ends of the machines have to be sealed from the surrounding environment as much as possible. The fundamental challenge is to provide a reliable seal on the rotating parts in the machine housing. One of the most effective options is the dry gas seal. This technology is based on a rotating and a non-rotating ring being separated by a very thin film of fluid. The gap between the two rings is a few micrometers at design operating conditions. Therefore, a small amount of leakage across the rings arises. Despite the many advantages, dynamic gas seals have some disadvantages. Due to their design, they can only reduce the pressure radially from the outer diameter to the inner diameter and require grooves on the rotating ring to ensure a stable operation during transit conditions, e.g. lift off beyond the design criteria. Furthermore, they are very sensitive to particles in the flow, such as oil contamination or vibrations, due to the very small gaps.

The aerostatic dry gas seal presented in this paper has a similar structure and function to an aerodynamic dry gas seal. In contrast to conventional dry gas seals, aerostatic versions require no grooves on the rotating ring. An example of an aerostatic dry gas seal is illustrated in Fig. 1. As a result of the aerostatic effect, the sealing surface lifts off and forms a gap of the order of a few micrometers. To ensure that this gap is formed, an aerostatic pressure field has to be generated between the seal rings. In order to obtain a controlled pressure field in the gap, the sliding ring is made of a porous material. Consequently, the through flow is regulated and a controlled pressure distribution is obtained in the gap between the two rings.

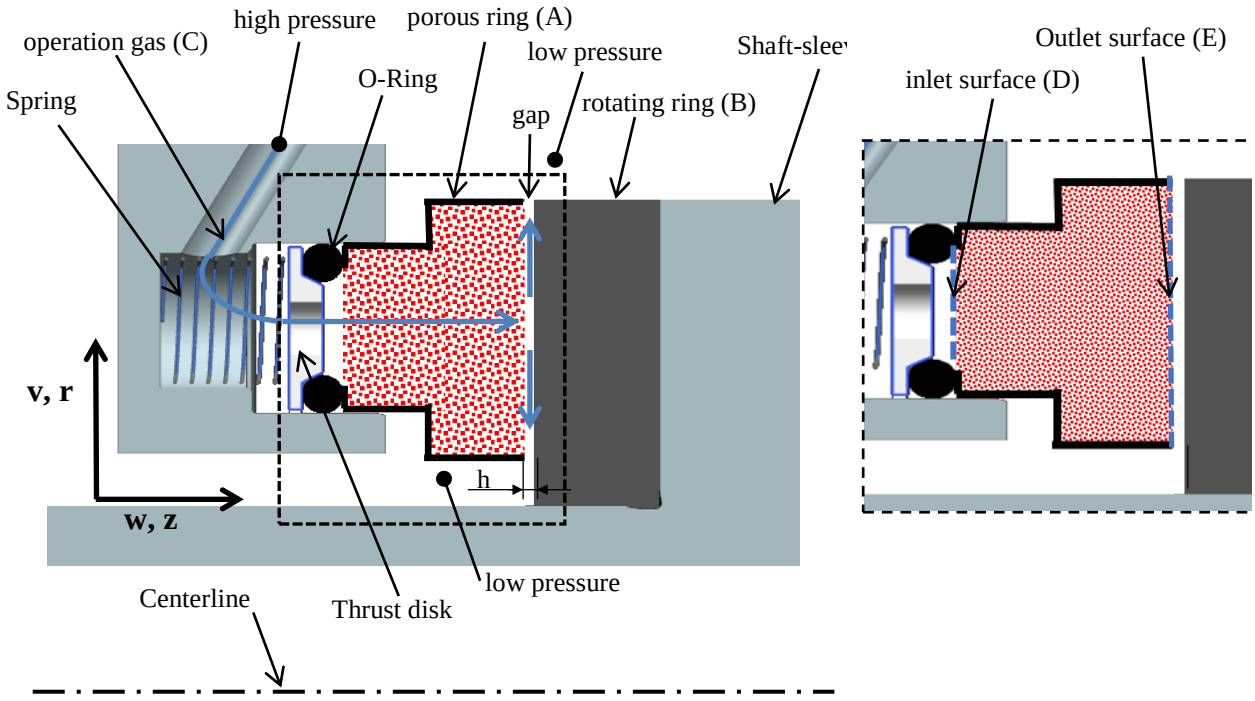

Figure 1: Aerostatic Dry Gas Seal

In the unpressurized state the porous ring (A) is pushed by the spring against the rotating ring (B). By applying a pressure to the inlet (C), the porous ring which is connected to the inlet bore is pressurized by an operation gas. Initially, the same pressure exists at the inlet surface (D) and the outlet surface (E) of the porous ring. As the outlet surface is larger than the inlet surface, the porous ring is pushed in the negative z-direction (Fig. 1) against the spring and a gap is formed. With increasing gap height, the pressure inside the gap decreases while the pressure at the inlet surface side remains almost constant. Hence, the aerostatic opening force decreases with increasing lift of the ring until a force equilibrium in the axial direction is established.

STATE OF THE ART

Aerostatic air bearings are very similar to aerostatic seals. Both systems provide a fluid film between a stationary and a rotating plane. The first investigations into radial bearings were reported in the study by Montgomery and Sterry (Montgomery & Sterry, 1955). Research into porous media had already begun in the middle of the 19th century. The experimental investigations of Darcy (Darcy, 1856) set the first basis for the formulation of empirical momentum balances. According to his observations of the flow of water through a vertical homogeneous sand bed, a linear relationship between the pressure gradient and the flow velocity relative to the open-tube cross-section u_0 exists:

$$-\frac{\partial p}{\partial z} = \frac{\eta}{K} u_0 \tag{1}$$

When considering the dynamic viscosity η, the permeability K can be defined as a proportionality constant. The application of Darcy`s law is limited to laminar flows in which the friction forces dominate. This is also referred to as a "viscous flow". An increase in the flow velocity leads to an increase in the inertial forces until they dominate ("inertial flow"). At this point, a turbulent flow arises which would obey the Forchheimer equation. The main focus of this field of research is on transport processes within porous media and their micro- and macroscopic modeling. Dagan (Dagan, 1989), Dullien (Dullien, 1992) and Hilfer (Hilfer, 1996) give an overview of the ways in which pore structures can be implemented in a mathematical model and how crucial this is for the results.

Heinzl and Zehentbauer (Heinzl & Zehentbauer, 1990) investigated the influence of the densification of the porous surface in an air bearing on its permeability and the bearing characteristics. Despite production difficulties in manufacturing, the study showed an improved pressure build-up in the narrow gap. In 1991, Hopfner (Hopfner, 1991) compressed a sintered bronze bearing in order to avoid the manufacturing problems with rollers. Gerke (Gerke, 1991) used Hopfner 's work as a basis for his research in 1991, which introduced a series of approximations for the design of porous air bearings. He established a high basic load factor with very small gaps.

Since the beginning of last century, one main focus of research has been the theoretical analysis of fluid flow in narrow gaps and the interaction of the fluid with stators and rotors. The study conducted by Muijderman E.A. (Muijderman, 1964) was the first fundamental step for modern numerical approaches describing a fluid flow in a spiral groove bearing with a narrow gap. Most of the approaches for describing fluid films within narrow gaps are based on the Reynolds theory of lubrication developed in the late 19th century. Reynolds' approach simplifies the equations of a continuum flow in such a way that the pressure distribution in the fluid film can be calculated based upon its dependence on a few characteristic parameters. To solve the Reynolds equation three numerical methods can be considered: Finite Volume (FV), Finite Element (FE) and Finite Difference (FD).

In this paper, the Reynolds equation is solved with the FD-method, due to the simplicity of the geometry (of the porous ring and the gap) as well as the numerical advantages over the other numerical methods.

EQUATIONS AND METHODOLOGY

The equations to be solved are based on the Reynolds theory and Darcy`s law to calculate the pressure profile in the gap and the pressure distribution in the porous ring. This theory is derived from the Navier-Stokes equation and the continuity equation plus additional assumptions (see (Lebeck, 1991), (Szeri, 2011), (Frene, 2005), (Bear, 1972)):

- The fluid viscosity is constant
  - Pressure range 0 – 2 barg
  - Temperature range 20 °C - 30 °C

- The fluid is considered to be Newtonian
- Laminar flow exists between the rings
  - The lubrication inertia in the narrow gap is neglected

In the porous volume Darcy`s equation can be written as follows:

Axial velocity:

$$w(z) = -\frac{K_i}{\eta}\frac{\partial p}{\partial z} \tag{2}$$

Radial velocity:

$$v(r) = -\frac{K_j}{\eta}\frac{\partial p}{\partial r} \tag{3}$$

In a narrow gap, the film thickness is small in relation to the other dimensions. Therefore, the velocity gradients in the radial direction are the only significant gradients. The rotating ring has no grooves and can therefore be regarded as hydraulically smooth. Additionally, it is assumed that no turbulence or vortices develop in the flow and that laminar fluid flow is present. Viscosity, pressure and temperature are presumed to be constant across the thickness of the film. The velocity at the walls is set to zero due to the adhesive condition (non-slip flow).

For the narrow gap, the Navier-Stokes equation is simplified based on the listed assumptions as show in equation (4).

$$\frac{\partial p}{\partial r} = \eta\frac{\partial^2 v}{\partial z^2} \tag{4}$$

By integrating equation (4) twice with respect to z, and substituting the velocities into the boundary conditions, constants of integration are established. The velocity distribution obtained is:

$$v(r,z) = \frac{1}{2\eta}\frac{\partial p}{\partial r}(z^2 - zh) \tag{5}$$

Thus, the velocity of the fluid depends on pressure and film thickness. In this paper the density is also considered as a variable. The consideration of the continuity equation for compressible fluids is given as follows:

$$\frac{\partial \rho}{\partial t} = div(\rho \cdot \vec{c}) \tag{6}$$

The process is assumed to be isothermal. This yields the following equation for an ideal gas:

$$\frac{p}{\rho} = const. \tag{7}$$

In the continuity equation (6), the velocities integrated over the height of the gap h are used. The density is described by means of the Boyle-Mariotte equation (7) by as a function of pressure. Finally, steady state equations are derived and written as follows:

For the porous domain:

$$r\frac{\partial}{\partial r}\left(-\frac{K_j}{\eta}\frac{\partial p}{\partial r}\right)+\frac{\partial}{\partial z}\left(-\frac{K_i}{\eta}\frac{\partial p}{\partial z}\right)=0 \tag{8}$$

For the gap domain:

$$r\frac{\partial}{\partial r}\left(ph^3\frac{\partial p}{\partial r}\right)+\frac{\partial}{\partial z}\left(-\frac{K_i}{\eta}\frac{\partial p}{\partial z}\right)=0 \tag{9}$$

NUMERICAL APPROACH

To determine the pressure profile in the gap, equations (8 & 9) must be solved at each individual grid point in the porous ring as well as in the gap. In Fig. 2, a two-dimensional calculation grid is shown and applied to the porous ring. Due to the simplifications that are made, i.e. that the film thickness is small in relation to the other dimensions, only one node in the axial direction can be used in the gap. The mass flows for each node and its structures are shown in Fig. 2. The result of the calculation in the porous ring of the outlet surface is a boundary condition for the calculation of the pressure field in the gap. Therefore, the last cell in the porous ring is the intersection of the two domains.

The nodes are numbered in both directions by means of indices. In the axial direction they are marked with i and in the radial direction with j. The numbering scheme and the distribution of the calculation grid are shown in Fig. 2. The yellow part (left in the porous ring, I) is the porous medium and the green part (right cell, II) is the gap.

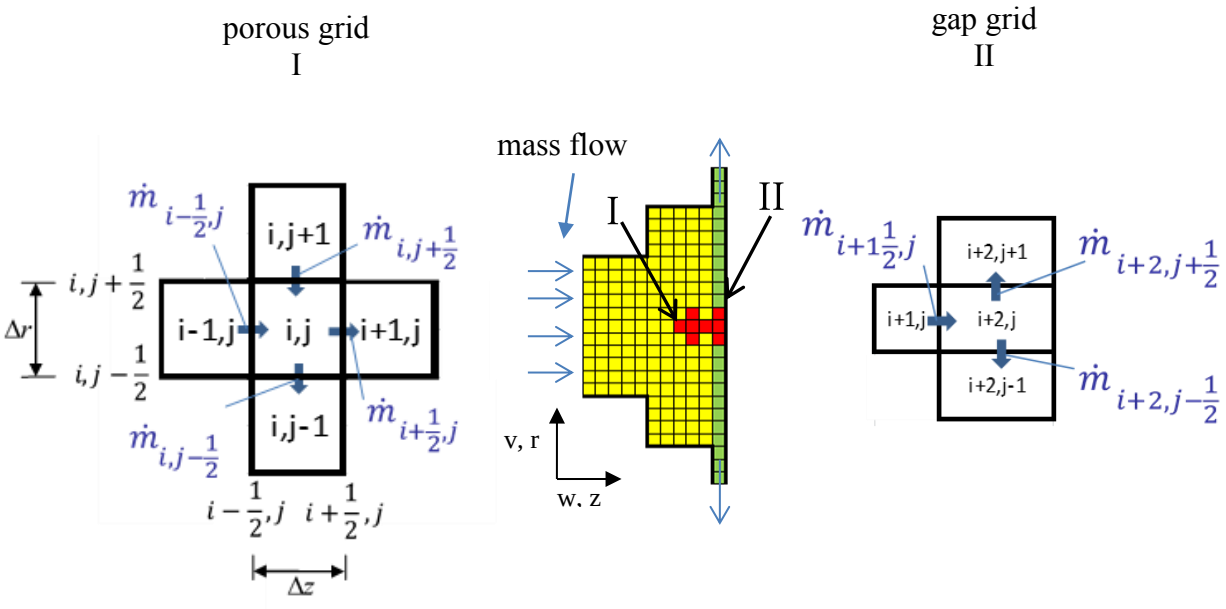

Figure 2: Two-dimensional calculation grid

For the finite difference method, equations (10 & 11) are written as given below. The parameters of each node can be described using the information from the neighboring nodes. The continuity of the mass flow is represented for each discretized volume element.

In the porous domain:

$$\frac{p}{RT}\frac{K_i}{\eta}\frac{\partial p}{\partial z}\pi\left(r^2_{i,j+\frac{1}{2}}-r^2_{i,j-\frac{1}{2}}\right)\frac{\Delta\varphi}{360°}-\frac{p}{RT}\frac{K_i}{\eta}\frac{\partial p}{\partial z}\pi\left(r^2_{i,j+\frac{1}{2}}-r^2_{i,j-\frac{1}{2}}\right)\frac{\Delta\varphi}{360°}+\frac{p}{RT}\frac{K_j}{\eta}\frac{\partial p}{\partial r}2\pi r^2_{i,j+\frac{1}{2}}\Delta z\frac{\Delta\varphi}{360°}-\frac{p}{RT}\frac{K_j}{\eta}\frac{\partial p}{\partial r}2\pi r^2_{i,j-\frac{1}{2}}\Delta z\frac{\Delta\varphi}{360°}=0 \tag{10}$$

In addition, in the gap domain:

$$-\frac{p}{RT}\frac{K_i}{\eta}\frac{\partial p}{\partial z}\pi\left(r^2_{i,j+\frac{1}{2}}-r^2_{i,j-\frac{1}{2}}\right)\frac{\Delta\varphi}{360°}+\frac{p}{RT}\frac{h^3}{12\eta}\frac{\partial p}{\partial r}2\pi r_{i+2,j-\frac{1}{2}}\frac{\Delta\varphi}{360°}+\frac{p}{RT}\frac{h^3}{12\eta}\frac{\partial p}{\partial r}2\pi r_{i+2,j+\frac{1}{2}}\frac{\Delta\varphi}{360°}=0 \tag{11}$$

To calculate the pressure at the node i, j, the information of the 4 neighboring nodes of the grid i+1, i-1, j+1, j-1 is used. Because equations (10 & 11) for ${p_{i,j}}^2$ are nonlinear, a quasilinear form which can be solved numerically is required by applying the Newton method. Using $\xi = {p_{i,j}}^2$ the following linear equations are obtained:

In the porous domain:

$$K_i\frac{1}{2}\frac{\left(\xi_{i-1,j}-\xi_{i,j}\right)}{\Delta z}\left(r^2_{i,j+\frac{1}{2}}-r^2_{i,j-\frac{1}{2}}\right)-K_i\frac{1}{2}\frac{\left(\xi_{i,j}-\xi_{i+1,j}\right)}{\Delta z}\left(r^2_{i,j+\frac{1}{2}}-r^2_{i,j-\frac{1}{2}}\right)+K_j\frac{\left(\xi_{i,j+1}-\xi_{i,j}\right)}{\Delta r}r_{i,j+\frac{1}{2}}\Delta z-K_j\frac{\left(\xi_{i,j}-\xi_{i,j-1}\right)}{\Delta r}r_{i,j-\frac{1}{2}}\Delta z=0 \tag{12}$$

In the gap domain:

$$\frac{h^3}{6}\frac{\left(\xi_{i+2,j}-\xi_{i+2,j+1}\right)}{\Delta z}r_{i+2,j-\frac{1}{2}}+\frac{h^3}{6}\frac{\left(\xi_{i+2,j}-\xi_{i+2,j-1}\right)}{\Delta z}r_{i+2,j+\frac{1}{2}}+K_i\frac{1}{2}\frac{\left(\xi_{i+1,j}-\xi_{i+2,j}\right)}{\Delta z}\left(r^2_{i,j+\frac{1}{2}}-r^2_{i,j-\frac{1}{2}}\right)=0 \tag{13}$$

Once this has been achieved, it is possible to calculate the pressure field at the numerical grid points. The calculation is carried out in several iterative steps on the basis of the previously calculated step. Thus, the equations can be written as follows:

In the porous domain:

$$\xi^{n+1}_{i,j}=\frac{1}{A_{i,j}}\left(\xi^n_{(i-1,j)}B_{i,j}+\xi^n_{(i+1,j)}C_{i,j}+\xi^n_{(i,j+1)}D_{i,j}+\xi^n_{(i,j-1)}E_{i,j}\right) \tag{14}$$

In the gap domain:

$$\xi^{n+1}_{i+2,j}=\frac{1}{F_{i,j}}\left(\xi^n_{(i+2,j+1)}G_{i,j}+\xi^n_{(i+2,j+1)}H_{i,j}-\xi^n_{(i+2,j-1)}M_{i,j}\right) \tag{15}$$

The matrix form containing all grid points can be described as follows:

$$M\cdot\xi^n_p=\xi^{n+1}_p \tag{16}$$

Here, M is the coefficient matrix, ξ_p^n is a vector with the pressure of the surrounding nodes and ξ_p^{n+1} is a vector with the pressure of the desired nodes. The iteration takes place until the defined convergence criterion is reached.

The convergence criterion is described as follows:

$$\varepsilon = \frac{\left|\xi_{i,j}^{n+1} - \xi_{i,j}^{n}\right|}{\xi_{i,j}^{n}} \leq \varepsilon_0 = 10^{-6} \tag{17}$$

with ε_0 being the required convergence accuracy.

PERFORMANCE PARAMETERS

The opening forces and closing forces that occur during operation are shown in Fig. 3.

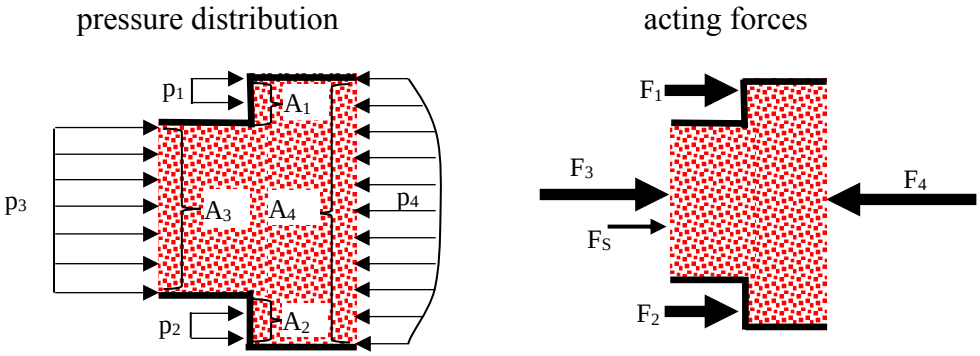

Figure 3: Pressure distribution and forces

After the pressure distribution has been calculated, the opening force is determined according to equation (18) as follows:

$$F_o = F_{open} = \int_A pdA = \int_{ri}^{ra} 2\pi p_4(r) r dr \tag{18}$$

The closing force which consists of three pressure forces and a spring load is proportional to the opening force as follows:

$$F_{o,sp} = \frac{F_{open}}{\mathrm{F}_{close}} \tag{19}$$

Performing an iterative process, the gap height is varied until force equilibrium is reached.

RESULTS

Based on preliminary investigations on a prototype of the porous ring, an area ratio A_3/A_4 of around 0.7 (entrance area to exit area) is chosen as the geometric parameter for the simulation. Calculations with a homogeneous and controlled permeability are performed and presented. As the self-adjusting ring is crucial for the function of the seal, the focus is put on the dependence of the force equilibrium on the size of the gap.

After a preliminary study of grid independence and ensuring consistent results for the numerical calculation, a grid of 3170 nodes is used. As shown in Fig. 2, this is divided into a porous (yellow) and a gap domain (green). Due to the boundary conditions and the small pressure change across the ring, fewer nodes are needed in the axial direction. In the porous part, 20 axial and 150 radial nodes are utilized. The gap height is very small in comparison to the length and width of the lubrication gap, whereby the speeds can only be considered radially and thus only one node in the axial direction in the gap is sufficient. Therefore one node in the axial direction, 150 nodes in front of the porous ring and 10 nodes each at the edges of the ring are arranged in the radial direction in the gap.

The boundary conditions and the permeability of the geometry for the numerical investigations in this study are given as follows:

- Operating pressure = 3 bar
- Ambient pressure = 1 bar
- Permeability = 10^{-13} m^2

DETERMINATION OF FORCE

First, the "lift off" situation is considered. In this case, the seal is subjected to an inlet pressure and the pressure profiles in the gap are calculated for different gap heights. The pressure versus the normalized radius of the sealing gap is plotted in Fig. 4.

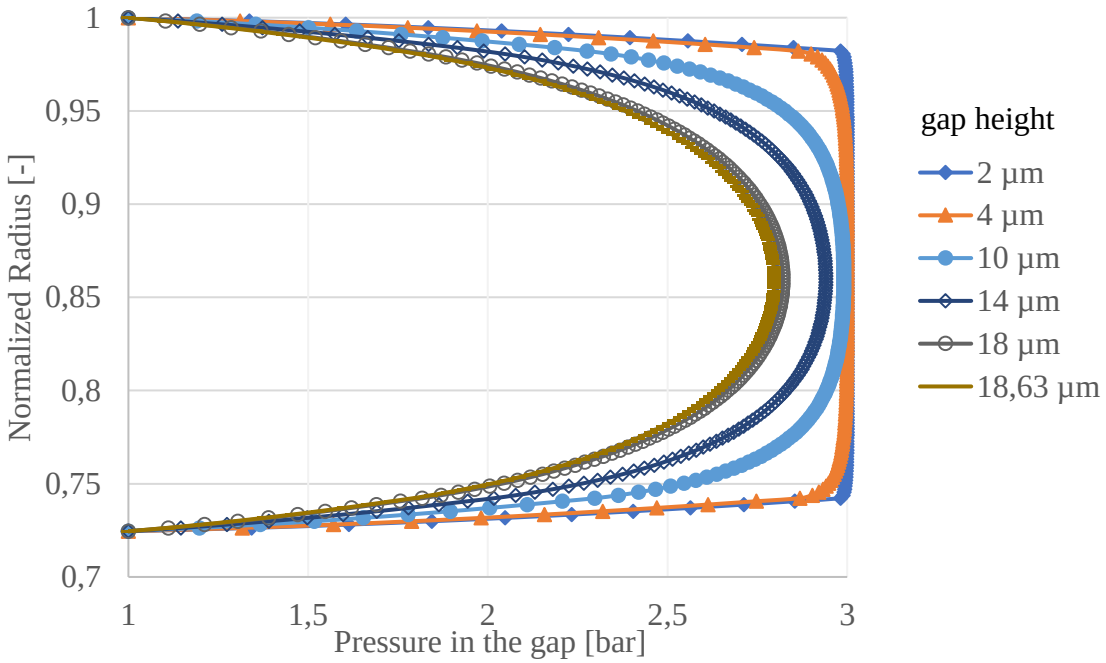

Figure 4: Lift off: Pressure distribution at different gap heights for 3 bar operating pressure

The figure clearly shows that the pressure decreases towards the borders of the ring with increasing gap height, while a reduction of the resulting opening force on the porous ring in the gap is observed for the same operating pressure.

The resulting opening force is plotted together with the closing force versus the gap height in Fig. 5. The horizontal line represents the closing force which is composed of the pre-compression and reaction force of the spring. The intersection of the two lines represents the gap height at force equilibrium.

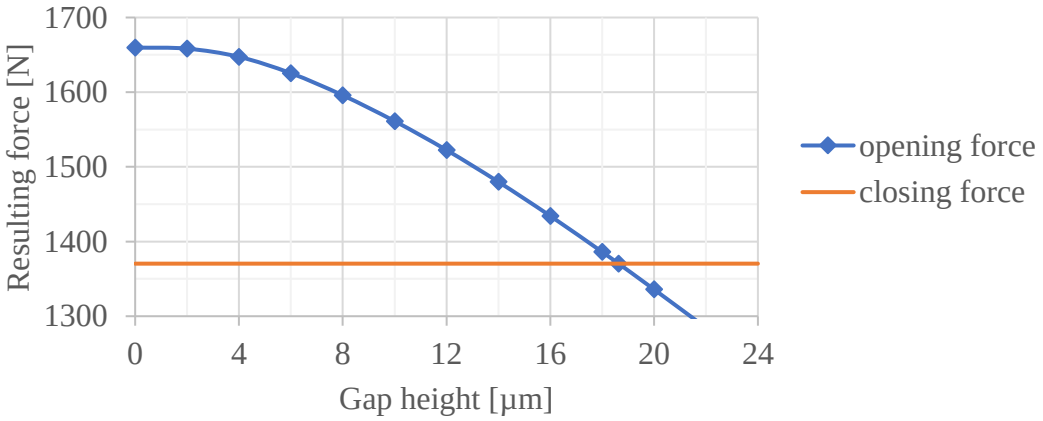

Figure 5: Force balance: opening force and closing force versus gap height

Under the given circumstances and boundary conditions, the gas seal reaches its force equilibrium at 18.63 micrometer gap height.

INFLUENCE OF POROSITY DISTRIBUTION

In Fig. 6, the pressure distribution is shown in the porous part of the seal as well as in the gap in the case of force equilibrium. To improve clarity, the height of the gap is enlarged by a factor of 100 in the graphical representation.

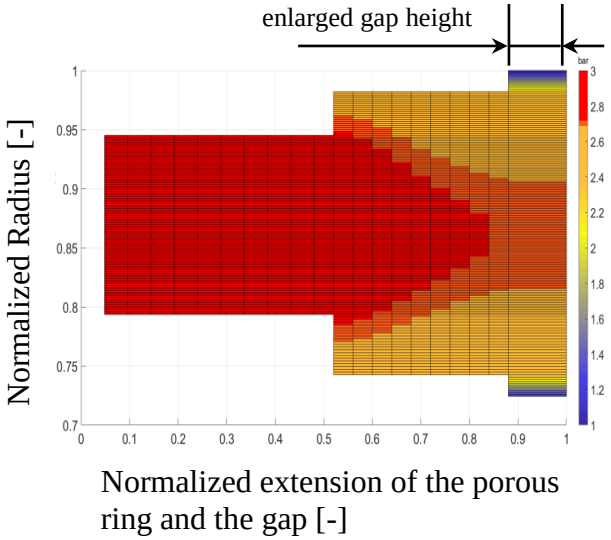

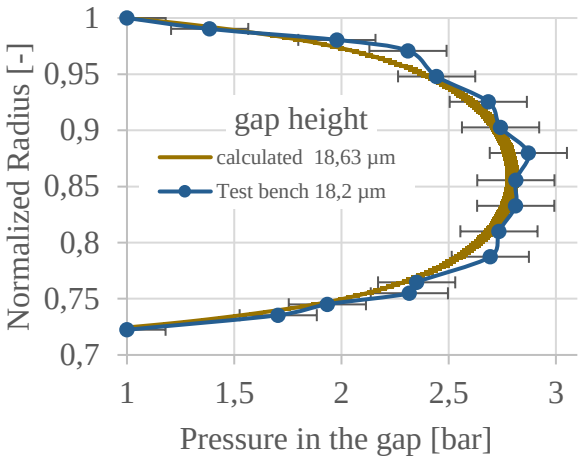

Figure 6: Pressure distribution in the porous ring and in the gap

Figure 7: Calculated and measured pressure profiles in the gap at force equilibrium

In the first calculation, the permeability of the porous ring is kept constant in both the radial and axial directions. Fig. 7 shows the pressure profile in the gap at force equilibrium. It illustrates a reaction in the pressure profile of the porous ring caused by the pressure profile in the gap. As a result, the pressure profiles in both the gap and the porous material significantly depend on each other. In order to validate the calculation, a prototype of the porous ring with constant permeability was manufactured and the pressure distribution in the gap was measured in a test bench. Due to simplifying assumptions for the calculation, the measured and calculated results do not exactly agree with each other. In addition, the measurement errors and the manufacturing tolerances of the test bench lead to further deviations from the calculated results. The gap measured during the experimental test is noticed to be smaller than the numerical result under the same boundary conditions.

Due to the pressure loss in the porous ring, less pressure in the gap is available for gap generation. To keep the acting forces in equilibrium, the gap between the rings is reduced. Thus, the leakage flow decreases and the static pressure increases. Due to the unchanged boundary conditions, the equilibrium of the forces arises at a smaller gap height.

In the next step, the permeability in the radial direction is varied. In Fig. 8a, the permeability increases with increasing radius, while in Fig. 8b, the permeability decreases with increasing radius. For comparability, it is crucial to keep the average permeability and the area of the respective permeability constant. Otherwise the gap height changes under the same boundary conditions.

a)

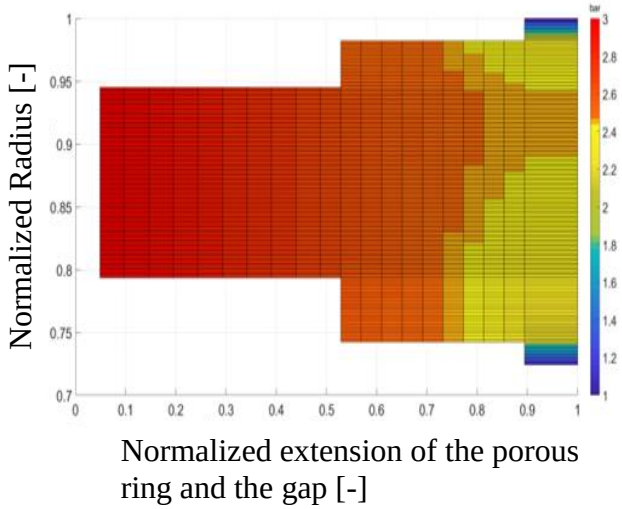

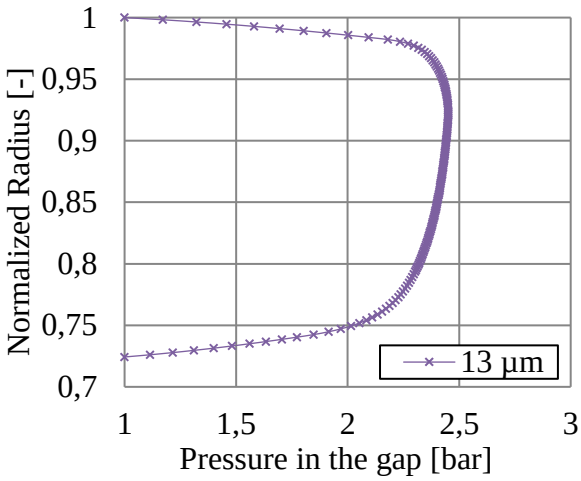

b)

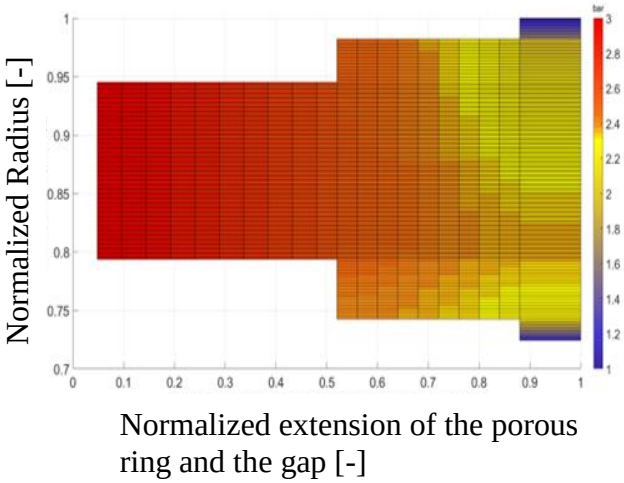

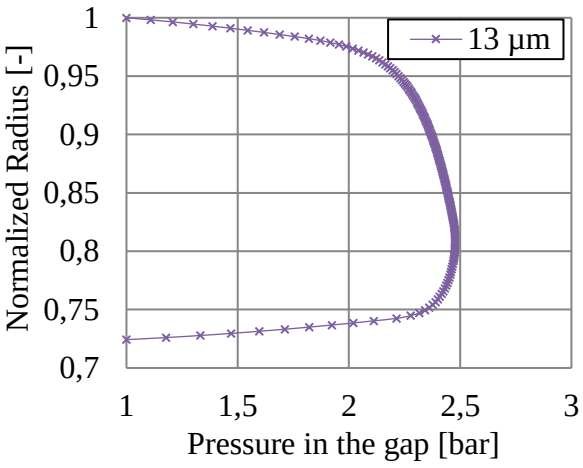

Figure 8: Pressure distribution in the porous ring with varied permeability

Figure 9: Pressure profiles in the gap with varied permeability

The chosen permeability allocation causes asymmetric static pressure distributions resulting from the flow velocity caused by the different pressure drops in the porous ring. The increase of local pressure results in a different distribution of forces on the outlet surface of the porous ring at the same gap height. Due to the asymmetric pressure distribution in this case, the resulting aerostatic force does not occur at the middle position of the ring. If this force is sufficiently high, tipping of the ring may occur which can result in a deformed gap. However, the operating pressure used in this study is low, thus this effect can be neglected.

Fig. 9 shows the pressure profiles in the gaps when the permeability is varied as shown in Fig. 8a and 8b. It is obvious that the pressure distribution across the radius changes as a function of the permeability in the ring.

CONCLUSIONS

In this study, a two-dimensional domain has been used to determine the pressure profiles in a porous ring and in the narrow gap between the porous ring and the rotating ring for an aerostatic dry gas seal. In addition, Darcy's law and the Reynolds equation have been used to compute the pressure distribution in the gap. The variation of the gap height demonstrates the self-adjusting functionality of the seal. With increasing gap height, the aerostatic opening force decreases until the forces acting

on the seal ring are in equilibrium. A manufactured prototype has been used to validate the calculated results of a seal designed with constant permeability.

The pressure distribution in the seal gap can be influenced by variation of the permeability distribution of the porous ring. With a constant average permeability and a constant area for the respective permeability, the gap height should remain the same.

Test rings will be designed and manufactured in order to further validate the existing calculation tool experimentally to gain in-depth understanding into the determination of a permeability distribution which is able to control the leakage mass flow in the near future.

REFERENCES

Bear, J. (1972). Dynamics of fluids in Porous Media. Dover Publications, New York.

Dagan, G. (1989). Flow and transport in porous formations. Berlin: Springer.

Darcy, H. (1856). Les fontaines publiques de la ville Dijon. Victor Dalmont.

Dullien, F. A. (1992). Porous Media. Fluid Transport and Pore Structure. 2nd edn Academic Press Inc, San Diego.

Frene, J. N. (2005). Lubrification Hydrodynamique. Elsevier Science B.V.

Gerke, M. (1991). Auslegung von ebenen und zylindrischen aerostatischen Lagern bei stationärem Betrieb. Thesis, Technische Universität München.

Heinzl, J., & Zehentbauer, H. (1990). Neue Ergebnisse bei der Entwicklung aerostatischer Lager. Feinwerktechnik & Messtechnik 98 , pp. S.431-435.

Hilfer, R. (1996). Transport and relaxation phenomena in porous media. Prigogine, I., Rice, A. (Eds.), Adv. Chem. Phys. XCII. John Wiley & Sons.

Hopfner, J. (1991). Fertigung von aerostatischen Lagern aus poröser Sinterbronze mit oberflächenverdichteter Drosselschicht. Thesis, Technische Universität München.

Lebeck, A. O. (1991). Principles and design of mechanical seals.

Montgomery, G., & Sterry, F. (1955). A simple air bearing rotor for very high rotational speeds. In UK atomic energy research establ, pp. ED/R, volume 1671.

Muijderman, E. A. (1964). Spiral groove bearings. Thesis, Technological University Delft .

Szeri, A. Z. (2011). Fluid film lubrication. Cambridge University Press.